ELSEVIER

Journal of Materials Processing Technology 124 (2002) 366–371

Journal of Materials Processing Technology

www.elsevier.com/locate/jmatprotec

Numerical simulation of three-dimensional fiber orientation in short-fiber-reinforced injection-molded parts

K.-H. Han[b], Y.-T. Im[a,*]

[a]*Computer Aided Materials Processing Laboratory, Department of Mechanical Engineering, ME3227, Korea Advanced Institute of Science and Technology, 373-1 Kusong-dong, Yusong-gu, Taejon 305-701, South Korea*

[b]*Vehicle Development & Analysis Team, R&D Division, Hyundai Motor Co. & Kia Motor Corp., 772-1 Changduk-Ri, Namyang-Myun, Hwasung-Gun, Kyonggi-Do 445-850, South Korea*

Accepted 29 April 2002

Abstract

In this paper, a second-order orientation tensor, orientation average of dyadic product of orientation vector, was adopted to describe three-dimensional orientation distribution of short fibers in injection-molded parts. For calculation of the fiber orientation tensor, a closure approximation is needed to reduce the higher fourth-order orientation tensor to the lower second-order. A modified hybrid closure approximation, which can accurately describe random-in-space, random-in-plane, and uniaxial distribution of fiber orientations, is introduced to yield better computational results than existing solutions available in references. Comparisons between numerical calculations of the second-order orientation tensor and the orientation distribution function (ODF) in simple flow field were made in order to demonstrate the accuracy of the closure approximation proposed. Orientation tensor equation currently introduced was incorporated into a finite-element/finite-difference program for injection molding analysis. In addition, new numerical technique was developed to reasonably calculate velocity gradients using constant velocity elements. The developed program was applied to simulation of injection molding for the thin cavity of a sector of spherical shell. The analysis showed that the currently proposed numerical approach enhances the solution accuracy of fiber orientation prediction in injection-molded parts made of short-fiber-reinforced thermoplastics.

Keywords: Fiber orientation; ODF; Finite-element program

1. Introduction

Fiber orientation, which has a large effect on mechanical properties of injection-molded parts made of short-fiber-reinforced thermoplastics, greatly changes during processing. For effective production of such products, it is essential to predict such a flow-induced variation of fiber orientation. Therefore, many investigations have been carried out so far due to importance of the problem for predicting fiber orientation distribution. Jeffery [1] has derived the equation of orientation change of an ellipsoidal particle immersed in a homogeneous flow field-based on hydrodynamics. Folgar and Tucker [2] have added a diffusion term to Jeffery's equation in order to consider the interactions among fibers. Advani and Tucker [3] have introduced fiber orientation tensors, the moments of orientation distribution function (ODF) to describe fiber orientation. In this approach, only a few components are required to represent the state of orientation at each spatial point. This advantage has made the orientation tensor, especially the second-order tensor, to be widely used in the calculation of fiber orientation in flow molding processes [4,5].

In the present investigation, numerical simulation of three-dimensional fiber orientation distribution in injection molding was carried out. Second-order fiber orientation tensor was adopted to describe fiber orientation efficiently similar to the approach proposed by Advani and Tucker [3]. A weakness of this approach is that a fourth-order tensor must be approximated as a known second-order tensor to solve the governing equation. A modified hybrid closure approximation, which can accurately describe random-in-space, random-in-plane, and uniaxial distribution of fiber orientation, is proposed for better predictions.

The goal of this investigation is to improve the solution accuracy in simulation of fiber orientation distribution during injection molding in couple with simulation program for filling studies. For this purpose, fiber orientation routine was incorporated into the finite-element/finite-difference program developed by the authors [6]. The effect of fiber orientation

* Corresponding author.
E-mail address: ytim@mail.kaist.ac.kr (Y.-T. Im).

0924-0136/02/$ – see front matter
PII: S0924-0136(02)00255-8

upon flow field was neglected, assuming the thickness of the cavity is thin enough. In numerical implementation, velocity gradients, which should be determined in solving orientation tensors, were obtained by averaging the values for the surrounding control volume (CV) of each node to minimize numerical errors. Simulation was carried out for the thin cavity of a sector of spherical shell with three-dimensional geometry. The simulation results are compared well to demonstrate the improvement of solution accuracies.

2. Fiber orientation

Orientation of a single short fiber can be represented by unit vector $\mathbf{p} = (p^1, p^2, p^3)$. Considering numerous short fibers, the three-dimensional fiber orientation distribution can be approximated by orientation distribution function (ODF: $\psi(\mathbf{p})$) which is described as a probability density function of fiber orientation distribution. In order to use such a description of ODF in numerical calculations, a great deal of effort is required to determine ODF values in every directions at each spatial point. However, the orientation tensor as defined in the following can greatly reduce such efforts.

$$\text{second-order}: \quad a_{ij} = \oint_S p_i p_j \psi \, \mathrm{d}A, \tag{1}$$

$$\text{fourth-order}: \quad a_{ijkl} = \oint_S p_i p_j p_k p_l \psi \, \mathrm{d}A. \tag{2}$$

Here, S denotes the surface of unit sphere. The fiber orientation distribution can be effectively visualized by using eigenvalues and eigenvectors of a_{ij} as shown in Fig. 1. By definition, orientation tensors are symmetric in its indices and have the following normalized properties.

$$a_{kk} = 1, \tag{3}$$

$$a_{ijkk} = a_{ij}. \tag{4}$$

Repeated indices indicate summation unless otherwise specified. Because of such properties the second-order orientation tensor has only five independent components to consider at each spatial point.

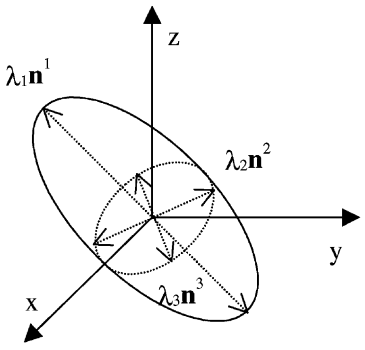

Fig. 1. Schematic representation of orientation distribution by second-order orientation tensor.

The governing equation of the second-order orientation tensor which will be used in this investigation is described by [3]:

$$\frac{\mathrm{D}a_{ij}}{\mathrm{D}t} = -\tfrac{1}{2}(\omega_{ik}a_{kj} - a_{ik}\omega_{kj}) + \tfrac{1}{2}\lambda(\dot{\gamma}_{ik}a_{kj} + a_{ik}\dot{\gamma}_{kj} - 2\dot{\gamma}_{kl}a_{ijkl}) + 2C_\mathrm{I}\dot{\gamma}(\delta_{ij} - 3a_{ij}), \tag{5}$$

where ω_{ij} and $\dot{\gamma}_{ij}$ are the components of vorticity and shear deformation rate tensor, respectively, with λ being a shape factor, C_I a fiber–fiber interaction coefficient and $\dot{\gamma}$ an effective shear rate. λ is defined as a function of aspect ratio r_e by

$$\lambda = \frac{r_\mathrm{e}^2 - 1}{r_\mathrm{e}^2 + 1}. \tag{6}$$

To solve Eq. (5), the fourth-order orientation tensor a_{ijkl} must be approximated as a function of the second-order orientation tensor a_{ij}. This closure approximation has a critical effect on the solution accuracy.

3. Modified hybrid closure approximation

In this section, a modified hybrid closure approximation, which is used in this investigation, is briefly introduced. For simplification, the problem was considered in the principal coordinate system of a_{ij}. Let λ_i be the ith eigenvalue and $\mathbf{n}^i = (n_1^i, n_2^i, n_3^i)$ be the ith eigenvector. Then the second- and fourth-order orientation tensors in this coordinate system, which are denoted by b_{ij} and b_{ijkl}, respectively, can be represented as follows:

$$b_{ij} = n_\mathrm{o}^i n_\mathrm{p}^j a_{\mathrm{op}} = \lambda_i \delta_{ij} \qquad (\text{no summation on } i), \tag{7}$$

$$b_{ijkl} = n_\mathrm{o}^i n_\mathrm{p}^j n_\mathrm{q}^k n_\mathrm{r}^l a_{\mathrm{opqr}}. \tag{8}$$

Without loss of generality, values of λ_1 and λ_2 should lie in the shaded region of Fig. 2 with the restriction of $\lambda_1 \geq \lambda_2 \geq \lambda_3$. The three points R_s, R_p and U represent the extremities of this region. At these extremities various

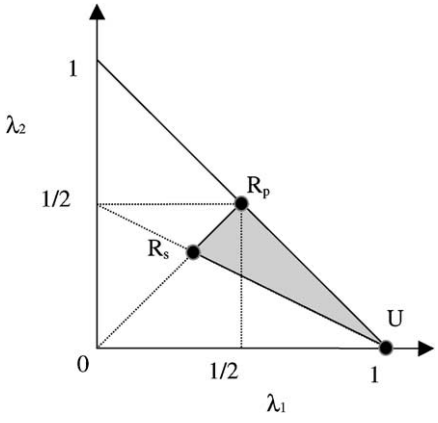

Fig. 2. Available region of eigenvalues in the λ_1 and λ_2 plane.

orientation distributions are possible, but in order to cover general cases it was assumed that the orientation distribution was random-in-space at point R_s, random-in-plane at R_p, and uniaxial at point U.

The main assumption introduced was that these conditions at three extremities should be satisfied for the closure approximation currently proposed. This closure approximation is defined as the modified hybrid closure approximation in the following.

3.1. Modified hybrid closure approximation—model I

The modified hybrid closure approximation—model I is defined by assuming, from the given second-order orientation tensor, an appropriate orientation distribution that exactly describes the one at the three extremities. It is reasonable that the orientation distribution should be expressed as simple as possible, e.g., egg-like near R_s, disk-like near R_p, and pen-like near U. At each region, ODF is defined to be symmetric in each coordinate plane, i.e., orthotropic, in order to cover general cases. The fourth-order orientation tensor, which was calculated from this ODF, has six non-zero components considering symmetries, i.e., b_{1111}, b_{2222}, b_{3333}, b_{1122}, b_{1133}, and b_{2233}. From the assumed ODF, b_{1111}, b_{2222}, and b_{3333} for the three extremities are derived as follows:

Egg-like ($\lambda_3 \geq 1/5$):

$$b_{1111}^{\text{egg}} = \tfrac{3}{35}(10\lambda_1 - 1), \qquad b_{2222}^{\text{egg}} = \tfrac{3}{35}(10\lambda_2 - 1),$$
$$b_{3333}^{\text{egg}} = \tfrac{3}{35}(10\lambda_3 - 1). \tag{9}$$

Disk-like ($\lambda_3 \leq 1/5, \lambda_1 \leq 3\lambda_2$):

$$b_{1111}^{\text{disk}} = \frac{1-s}{8}(7\lambda_1 - \lambda_2), \qquad b_{2222}^{\text{disk}} = \frac{1-s}{8}(-\lambda_1 + 7\lambda_2),$$
$$b_{3333}^{\text{disk}} = (3s)\lambda_3 \tag{10}$$

with $s = \lambda_3/(1 + 2\lambda_3)$.

Pen-like ($\lambda_3 \leq 1/5, \lambda_1 \geq 3\lambda_2$):

$$b_{1111}^{\text{pen}} = (1-r)(1-s)\lambda_1, \qquad b_{2222}^{\text{pen}} = (1-s)\lambda_2 - r(1-s)\lambda_1,$$
$$b_{3333}^{\text{pen}} = (3s)\lambda_3 \tag{11}$$

with $r = \lambda_2/(\lambda_1 + 3\lambda_2)$ and $s = \lambda_3/(1 + 2\lambda_3)$.

Other components b_{2233}, b_{1133} and b_{1122} can be determined from the normalized property.

Thus, modified hybrid closure approximation—model I can be defined as

$$a_{ijkl}^{\text{model I}} \equiv \begin{cases} a_{ijkl}^{\text{egg}} & \text{if } \lambda_3 \geq \frac{1}{5}, \\ a_{ijkl}^{\text{disk}} & \text{if } \lambda_3 < \frac{1}{5}, \lambda_1 \leq 3\lambda_2, \\ a_{ijkl}^{\text{pen}} & \text{if } \lambda_3 < \frac{1}{5}, \lambda_1 > 3\lambda_2. \end{cases} \tag{12}$$

3.2. Modified hybrid closure approximation—model II

As mentioned earlier, model I has an orthotropic property to be used for general cases. Thus, the idea was similar to the orthotropic closure approximation proposed by Cintra and Tucker [7]. They proposed two kinds of closure approximations, orthotropic smooth (ORS) and orthotropic fitted (ORF). ORS is described by linear interpolations of three extremities conditions and can be transformed into another kind of the modified hybrid closure as follows:

$$b_{1111}^{\text{ORS}} = -0.15 + 1.15\lambda_1 - 0.10\lambda_2,$$
$$b_{2222}^{\text{ORS}} = -0.15 + 0.15\lambda_1 + 0.90\lambda_2,$$
$$b_{3333}^{\text{ORS}} = 0.60 - 0.60\lambda_1 - 0.60\lambda_2. \tag{13}$$

Calculations based on model I usually underpredict the exact solutions of a_{ij}, while calculations based on ORS overpredict. Therefore, more accurate version of the modified hybrid closure approximation—model II was defined by coupling the results from model I and ORS as

$$a_{ijkl}^{\text{model II}} \equiv (1 - \text{FAC})a_{ijkl}^{\text{model I}} + \text{FAC} \cdot a_{ijkl}^{\text{ORS}}. \tag{14}$$

Interpolation factor FAC in this equation was found as a function of C_I by minimizing errors in selected flow fields as follows:

$$\text{FAC} = 0.52 - 0.9655 C_I^{1/2} \qquad (0 < C_I < 0.1). \tag{15}$$

For verification of closure approximations introduced, ODF (ψ) was solved directly and orientation tensors were calculated from Eqs. (1) and (2). The results were compared to solutions of the orientation tensor equation of Eq. (5) based on each closure approximation. In the current investigation, 'exact solutions' or 'exact values' imply 'computations determined by such an ODF'.

Comparisons of exact values and calculation results based on various closure approximations (hybrid (HYB) [3], ORS, ORF, model I, and model II) are shown in Fig. 3. Comparisons were made for simple shear flow assuming slender fiber particle ($\lambda = 1$) with $C_I = 0$ in Fig. 3(a) and $C_I = 0.01$ in Fig. 3(b). It can be seen that model II outperforms HYB, ORS, and model I as expected. In Fig. 3(b), both model II and ORF predict the fiber orientation better than the other closure approximations, while in Fig. 3(a) ORF underpredicts as time increases. This is because ORF was obtained from the exact solution with $C_I = 0.01$ and the fiber orientation prediction shows inaccurate behavior when C_I changes. If ORF was obtained by fitting ODF at various C_I values, then this specific error might decrease, but the overall errors increase. Model I gives better results than HYB when $C_I = 0$, while oscillation occurs when $C_I = 0.01$. Thus, it can be seen that model I guarantees better results only when $C_I = 0$, while model II being accurate for the whole range of C_I values. From such comparisons for selected flow fields, it was concluded that model II can be used in the simulation of fiber orientation distribution for general flow fields regardless of C_I values and can predict exact values better than existing closure approximations.

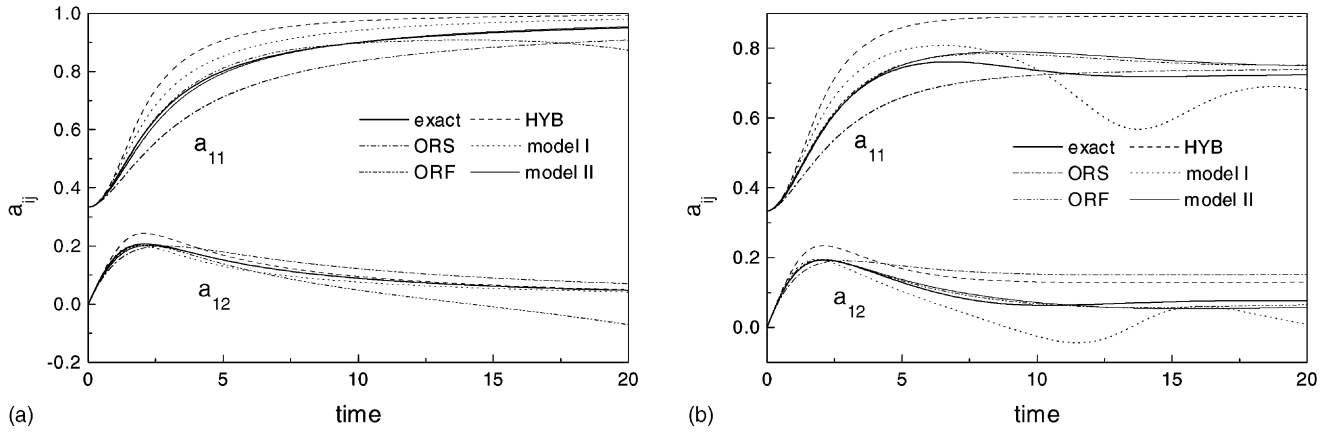

Fig. 3. Comparisons of a_{ij} between the exact solution and simulations for simple shear flow with: (a) $C_I = 0$ and (b) $C_I = 0.01$.

4. Numerical implementation with filling analysis

Numerical algorithm for predicting fiber orientations described earlier is incorporated into simulation program of filling study for injection molding [6]. The fiber orientation distribution was updated based on flow fields at each time step. The effects of fiber orientation upon flow fields were neglected in filling analysis.

In filling simulation, incompressible non-Newtonian and non-isothermal flow field was analyzed by employing lubrication approximation and hybrid of the finite-element/finite-difference method [8]. Linear triangular elements were used to describe thin cavity shape and the half thickness was divided into 10 uniform spacings which yielded 11 layers from the center to the cavity wall. At each time step, pressure field was calculated by the finite-element method in plane direction and temperature field by the finite-difference method in thickness direction. Velocity field was calculated from the information of pressure and temperature fields and used in advancing flow front automatically. Fixed-grid analysis enables simulation with complex cavity shape.

4.1. Calculation of velocity gradient

In solving Eq. (5), velocity, velocity gradient, and gradient of a_{ij} should be determined. Velocity gradient in thickness direction can be easily obtained from the flow formulation. However, special consideration should be given in calculating velocity gradients in plane direction, since linear pressure profile produces constant velocity. In several researches [4,5], nodal velocity was first determined by averaging velocities of surrounding elements. Velocity gradient at each element is calculated from this nodal velocity employing the same shape function of linear triangular element. But this procedure involves significant numerical errors. For example, velocity gradients calculated in this way cannot satisfy incompressibility requirement. Numerical test shows that the trace of shear rate tensor is of same order as the effective shear rate even if meshes are only slightly distorted.

Therefore, in this investigation, new numerical technique was developed to reasonably calculate velocity fields from the constant velocity element. The velocity gradient can be averaged in the CV according to the current approach as follows.

Fig. 4 shows node N and surrounding CV. Transforming the volume integration of velocity gradient in CV into surface integral on boundaries by divergence theorem, average velocity gradient at node N can be expressed by

$$[u_{j,i}]_N \cong \frac{1}{V_{CV}} \int_{CV} u_{j,i}\, dV = \frac{1}{V_{CV}} \int_{\partial CV} n_i u_j\, dA$$
$$= \frac{1}{\sum A_{SV}} \sum \left(\int_{\partial SV} u_j n_i\, ds + A_{SV} \frac{\partial u_j}{\partial z} \delta_{i3} \right), \qquad (16)$$

where SV denotes the portion of CV in each surrounding element, n_i the normal vector component, and V and A volume and area, respectively. This expression satisfies incompressibility since at each node mass conservation holds. In treating Eq. (16) in three dimension, special care must be given upon coordinate change between local and global system since the velocity component from filling simulations is given in local coordinate. Since velocity gradient is known at each node, a_{ij} can be easily calculated at each node. Spatial gradient of a_{ij} which is needed to treat material derivative in Eq. (5), is calculated at each element, and the results are averaged at each node.

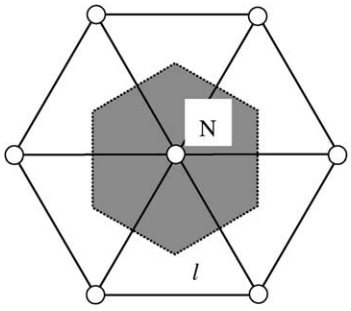

Fig. 4. Schematic diagram of CV (shaded region) of node N.

4.2. Initial and boundary conditions

Initially random distribution of fiber orientation was assumed. To solve Eq. (5), further consideration must be given at inlet and melt front nodes where spatial gradient of a_{ij} and velocity gradient cannot be normally obtained. In this investigation, random distribution was assumed at both positions. However, any other considerations such as flow aligned distribution at inlet or fountain flow effect at melt front, can be accommodated to effectively simulate practical molding processes.

At the lateral cavity wall, impermeability condition was imposed in calculating velocity gradient. However, no-slip condition, if necessary, can be easily imposed.

4.3. Numerical stability

For accurate determination of the orientation equation following two conditions must be satisfied.

$$\text{Courant number limit}: \quad \text{Co} = \frac{U\Delta t}{\Delta x} < 1, \tag{17}$$

$$\text{Jeffery number limit}: \quad \text{Je} = \dot{\gamma}\Delta t < 1, \tag{18}$$

where U and Δx denote characteristic speed and mesh size, respectively.

In this investigation, appropriate time step at each thickness layer was determined by satisfying Eqs. (17) and (18) and Eq. (5) is implicitly integrated by using the predictor–corrector method.

5. Application

Cavity shape for test simulation is shown in Fig. 5. This cavity is a sector of spherical shell of 5 cm radius with 2 mm thickness. For processing conditions, inlet and wall temperatures were set to 200 and 30 °C, respectively, and injection rate was set to 5.0 cm^3/s. Material properties used in the current simulation are as follows:

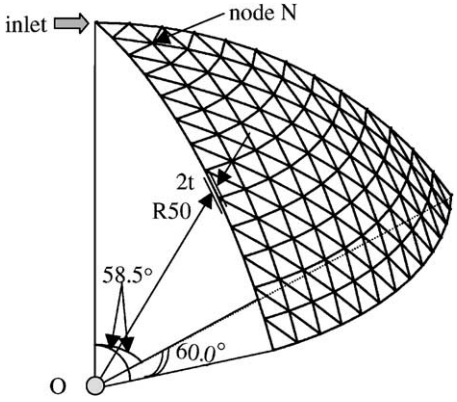

Fig. 5. Mesh layout for test simulation.

Density	727.6 kg/m^3,
Specific heat	2700 J/kg K,
Thermal conductivity	0.175 W/m °C,
Viscosity	$\eta(\dot{\gamma}, T) = \eta_0(T)/(1 + [\eta_0(T)\dot{\gamma}/\tau^*]^{1-n})$, $\eta_0(T) = B\exp(T_b/T)$ $(n = 0.204, \tau^* = 3.07\times 10^4\,\text{Pa}, B = 0.144\,\text{Pa s}, T_b = 4830\,\text{K})$,
For fibres	$\lambda = 1, C_I = 0$.

Injection molding simula-and (b). In these figures, a_{ij} tion using these informationsat each element was plotted was carried out. Fiber orienta-for visualization. At the first tion distributions at the first andlayer, fibers are oriented seventh layer at the end of fill-transversely except near the ing are represented in Fig. 6(a)gate and front since radially

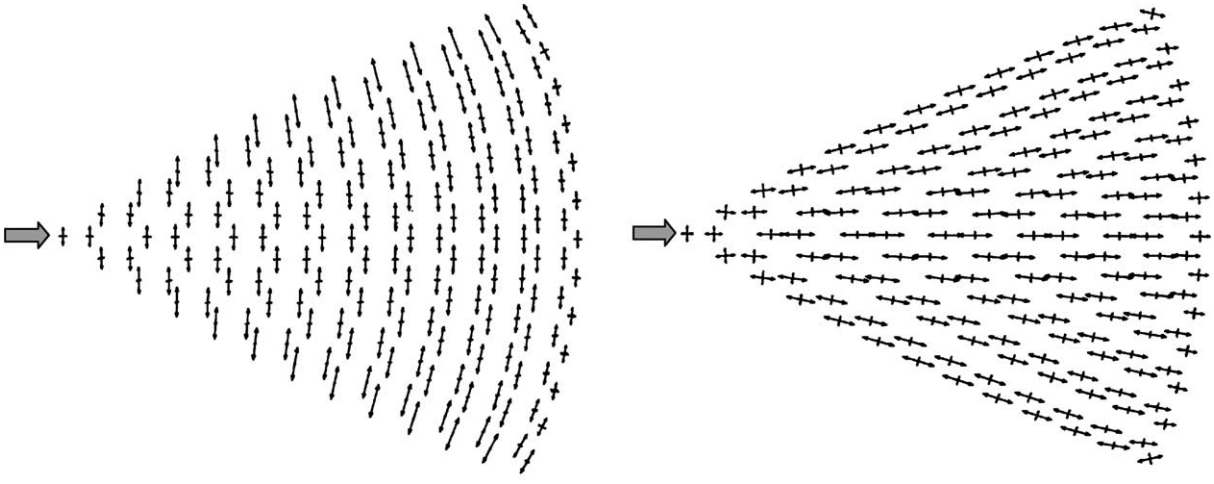

Fig. 6. Calculated fiber orientation distribution at the end of filling at the: (a) first layer and (b) seventh layer.

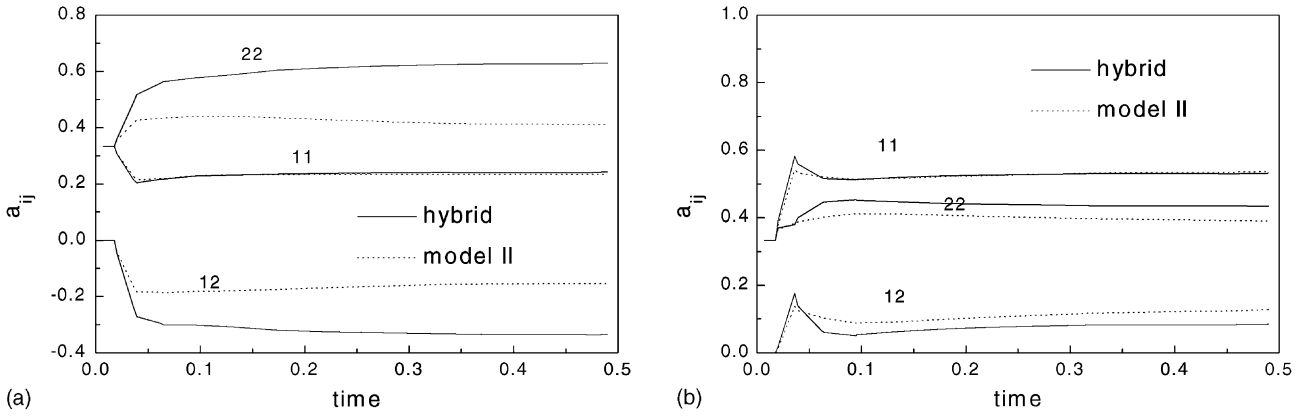

Fig. 7. Comparisons of simulation results using hybrid and model II at node *N* at the: (a) first and (b) seventh layer.

diverging flow is dominant, while being flow-aligned at the seventh layer since shear flow is dominant. Thus, it was found that numerical formulations developed in this study produced reasonable fiber orientations.

In order to look into the effect of closure approximation, simulations were carried out using hybrid closure approximation and model II (modified hybrid). The simulation results at node *N* of Fig. 5 are compared in Fig. 7(a) and (b). Both figures show significant differences. Difference is severer at the first layer where diverging flow is dominant. Though experiments are not considered in this investigation, it can be easily construed from this result that modified hybrid closure approximation enhanced prediction of fiber orientation distribution and mechanical properties of final molded parts.

6. Conclusions

In this investigation numerical methods to calculate fiber orientation distribution in injection-molded parts were developed based on the second-order tensor approach. The modified hybrid closure approximation was introduced for more accurate calculations. This closure approximation accurately describes random-in-space, random-in-plane, and uniaxial distribution of fiber orientation, and was found to predict distributions more accurately in selected flow fields. Fiber orientation routine was incorporated into filling simulation program which was based on the fixed-grid finite-element/finite-difference method.

New numerical technique was proposed to reasonably calculate velocity gradient from simulation results of filling study. Test simulation was carried out using three-dimensional thin cavity of a sector of spherical shell. General trend of fiber orientations was predicted fairly well. The computational results based on the modified hybrid closure approximation showed that the predictive capability of fiber orientation distribution in the molded parts was greatly enhanced under the present processing conditions.

Acknowledgements

The authors wish to thank the grant from Korea Science and Engineering Foundation through the Engineering Research Center for Net Shape and Die Manufacturing at Pusan National University under which this work was possible.

References

[1] G.B. Jeffery, The motion of ellipsoidal particles immersed in a viscous fluid, Proc. Roy. Soc. Lond. A 102 (1992) 161–179.
[2] F. Folgar, C.L. Tucker, Orientation behavior of fibers in concentrated suspensions, J. Reinf. Plast. Compos. 3 (1984) 98–119.
[3] S.G. Advani, C.L. Tucker, The use of tensors to describe and predict fiber orientation in short fiber composites, J. Rheol. 31 (1987) 751–784.
[4] M. Gupta, K.K. Wang, Fiber orientation and mechanical properties of short-fiber-reinforced injection-molded composites: simulated and experimental results, Polym. Compos. 14 (1993) 367–382.
[5] S.T. Chung, T.H. Kwon, Numerical simulation of fiber orientation in injection molding of short-fiber-reinforced thermoplastics, Polym. Eng. Sci. 25 (1995) 604–618.
[6] K.-H. Han, Y.-T. Im, Compressible flow analysis of filling and post-filling in injection molding with phase-change effect, Compos. Struct. 38 (1997) 179–190.
[7] J.S. Cintra Jr., C.L. Tucker, Orthotropic closure approximation for flow-induced fiber orientation, J. Rheol. 39 (1995) 1095–1122.
[8] C.A. Hieber, S.F. Shen, A finite-element/finite-difference simulation of the injection-molding filling process, J. Non-Newt. Fluid Mech. 7 (1980) 1–32.